

An exploration of the Kuramoto model

Mathematical background, links with physics and numerical
analysis

Renze Dijkhuizen, 4866177 - July 7, 2021

Delft University of Technology
Bachelor of Applied Physics and Applied Mathematics

Thesis committee:

Dr. J.L.A. Dubbeldam	TU Delft, supervisor
Dr. ir. J.M. Thijssen	TU Delft, supervisor
Dr. E. Pulvirenti	TU Delft, committee member
Prof. Dr. Y.M. Blanter	TU Delft, committee member

Contents

1	Introduction	4
2	Numerical analysis	5
2.1	Good practices when using SDEs	5
2.2	Integrators	5
2.2.1	Euler-Forward	6
2.2.2	Milstein	6
2.2.3	On higher order methods	7
3	Theory	8
3.1	Kuramoto's analysis	8
3.2	Phase transition for annealed noise	10
3.3	Synchronization phenomena for quenched noise	11
3.3.1	Stability analysis	12
3.3.2	Fractional synchronization	13
3.3.3	Synchronization requirements	15
3.3.4	Ring coupling	19
4	Ising and XY model	23
4.1	Ising model	23
4.2	XY model	23
4.2.1	The KT-transition	23
5	Discussion	27
5.1	Analytical results	27
5.2	Numerical accuracy	27
6	Conclusion	28
	References	29
	Appendix	30
	Proof of the Binder cumulant limit	30

Abstract

This work is a bachelor thesis featuring a collection of explorations of the Kuramoto model in the presence of noise in one and two dimensions. The model was explored analytically and numerically. It contains a study of literature and new analytical derivations.

An attempt to link the fraction of oscillators to the order parameter resulted in experience through the process of deriving the result, but a plot of the first few terms of this expansion showed it not being close. The assumption on which the expansion was based however was shown to be valid in simulations.

More successfully an upper bound on the probability of synchronization was found. This probability was found on a ring consisting of N oscillators, and verified of a ring of 3 oscillators. The results was a bound better than one that was already calculated, though the method of verification used was not ideal.

An analysis of the stability of solutions on this 3-ring resulted a visual representation of entrainment and an amount of stable solutions possible, which was 1.

This result was in accordance with the more general result following from the investigation of a system of coupled rings with arbitrary sizes of either ring. We then expanded this system to conclude that the stability of the entire system could be split into the stability of either ring and the possibility of having a solution for the linking phase difference.

We elaborated on general practices when numerically analyzing SDEs and integrations methods. The Kuramoto model proved to be kind in the sense that the Euler-forward and Milstein scheme coincided.

In a more physics-centered approach we studied the Ising and XY model. This prompted literature study on the Kosterlitz Thouless transition, through analysing the spin-wave Hamiltonian and the energy of free vortex of a pair of vortices.

We also then explored conservation of the vortex-pair behaviour in a noise including Kuramoto model, which verified a duality in partition functions as described in ref. [1].

1. Introduction

Modern life is filled with impulses which require quick attention, coming from constant pings from social media or for example traffic. This makes it seem as if life has a chaotic nature, which might well be considering the second law of thermodynamics. This law states that in any energy related process, total entropy will either stay the same or increase. In more simple words; everything that we see happening around us slowly, but irreversibly, introduces bits of chaos in the universe. Yet, there are some aspects of life showing order, one of which is synchronization.

Synchronization can be a powerful and beautiful phenomenon. Most have experienced it through for example walking in step with another person. This may seem like a small feat, but when done in large groups it has the power to destroy metal and concrete bridges [2], which is also why military troops break step when marching over a bridge.

A powerful example which lies closer to me is rowing together with others. Though synchronization in the boat can be somewhat difficult to achieve, the feeling and power it delivers propels the boat like no other technique¹.



Figure 1.1: Me, the rower closest to the camera, rowing with my crew. The boat type we rowed in for this regatta was quite slow, but working in sync helped us achieve a nice second place.

Perhaps the most beautiful example however of synchronization can be seen in fireflies. Some types of fireflies, particularly in south Asia, light up periodically. They blink six times and then wait for a bit. When the sun starts to set the fireflies start to shine. When it is fully dark the fireflies interact with the blinking of others and they synchronize. This effect causes bushes or trees to light up and can be best described with [a video of these fireflies synchronizing](#)².

Many more examples can be found with varying complexity, such as [metronomes on a moving plate](#)³, but also heart cells, magnetic spins via the XY model and electrical networks such as power grids [3]. Phenomena like these sparked mathematical and physical interest and led to the Kuramoto model, which we will investigate in this work.

This work will be divided into three parts. First, in chapter 2, we will discuss how to approach numerical analysis of stochastic differential equations. Secondly, in chapter 3, we will review and elaborate on literature on the subject. Furthermore we will do some derivations on probabilities of synchronization and stability for certain systems. Lastly, in chapter 4, we will establish a link with the aforementioned magnetic spins via the XY model.

¹Some research suggests anti-phase rowing might be quicker, this does not however allow the boat to set a rhythm which can be felt. The stroke cycle might be more efficient in motion, but extra energy is needed for focusing on rhythm which could also be used to move the boat faster. Furthermore, it requires elongated boats which reduces stiffness and increases drag.

²<https://www.youtube.com/watch?v=2IVBDDVP168>

³<https://www.youtube.com/watch?v=T581GKREuBo>

2. Numerical analysis

For numerical analysis a Python implementation of the Kuramoto model was used. This was achieved using the well-known package `numpy` implemented using the Milstein scheme. The code used for this can be found on GitHub [4].

2.1 Good practices when using SDEs

In this work we are dealing with an SDE (Stochastic Differential Equation). Working with these equations is different from working with deterministic differential equations. For this we will write out three good practices when implementing numerical analysis of an SDE in Python.

Ensure reproducible results SDEs are inherently random. This is a property which makes them interesting, but it might make comparing runs harder. This can be mitigated by setting a *seed*, through `numpy.random.seed(some number)` for example. This locks the pseudo-random number generators on some initial condition, which in turn makes it so that randomly generated numbers will come out the same between runs.

Generate random numbers beforehand Pieces of code take time to evaluate. Often people will generate random numbers at each timestep to then perform calculations with. It is more efficient however to generate a large collection of random numbers before iterating. This saves computation time at each individual timestep as the numbers need only be read from memory.

Do not use `scipy` The python library `scipy` is popular and used very often when evaluating differential equations. It however works with variable step sizes, which helps improve accuracy, but no step size information is relayed back to the user during the integration process. This makes cumbersome to use this library with SDEs, where the numerical evaluation of random numbers often depends on the stepsize used. It would save time to outright skip `scipy` and look for a different library, or to write an integrating script manually.

2.2 Integrators

It may seem strange that such a simple scheme as Euler-Forward is used, but when integrating an SDE some caution is required.

Lots of simulations as of writing this use a scheme which is at least as advanced as Runge-Kutta-4. Some more delicate simulations even resort to symplectic integrators, which are a whole topic on their own, ensuring some conserved quantities. These scheme have been tested and verified extensively, producing many great results, but their usefulness in SDEs is limited¹. This is because many schemes rely on the solution being sufficiently smooth, which is not true in general for SDEs (take Brownian motion for example).

Thus, we rely on different methods. Methods for integrating SDEs are classified as a weak or strong approximation, as is often the case with any probabilistic convergence.

Strong or weak approximation An approximation X^h of the random process X is said to be an n -th order strong approximation of X if for all $t \in [0, T]$,

$$\mathbb{E} [|X_t^h - X_t|] = \mathcal{O}(h^n).$$

It is said to be an n -th order weak approximation if for all $t \in [0, T]$,

$$\mathbb{E} [f(X_t^h)] - \mathbb{E} [f(X_t)] = \mathcal{O}(h^n)$$

¹This is true for most schemes used with deterministic differential equations. It might be possible to find a symplectic integrator for some SDEs, but finding them seems to be very hard.

for a sufficiently wide class of functions $f : \mathbb{R} \rightarrow \mathbb{R}$ (for example, $C_b^\infty(\mathbb{R})$).

As with many forms of probabilistic convergence, the weak approximation is best used when the distribution of the random process is of interest. For more detailed information it is best practice to resort to a strong approximation [5].

2.2.1 Euler-Forward

For a simple Euler-Forward integration of a function we use a first order Taylor polynomial to obtain

$$x[t + \Delta t] \approx x[t] + \Delta t \cdot f[x, t]$$

for the ODE $\dot{x}(t) = f(x, t)$.

If we then look at the SDE $\dot{x}(t) = \dot{W}(t)$, where W is a Wiener-process we find something else, using that $W(t) - W(s) \sim W(t - s) \sim \mathcal{N}(0, t - s)$ by definition of a Wiener process.

$$\begin{aligned} x[t + \Delta t] &= x[t] + \Delta x && = x[t] + \Delta W \\ &= x[t] + (W[t + \Delta t] - W[t]) && = x[t] + W(\Delta t) \\ &= x[t] + \mathcal{N}(0, \Delta t) && = x[t] + \sqrt{\Delta t} \cdot \mathcal{N}(0, 1) \end{aligned}$$

This is a very useful identity as white noise is defined as the time-derivative of a standard Wiener-process. Thus, when using Euler-Forward, we find that the integration step for the SDE $\dot{x}(t) = f(x, t) + \dot{W}(t)$ must be

$$x[t + \Delta t] = x[t] + \Delta t \cdot f[x, t] + \sqrt{\Delta t} \cdot \mathcal{N}(0, 1) \quad (2.1)$$

This leaves us with a strong approximation of order $\frac{1}{2}$, producing figures 2.1a and 2.1b.

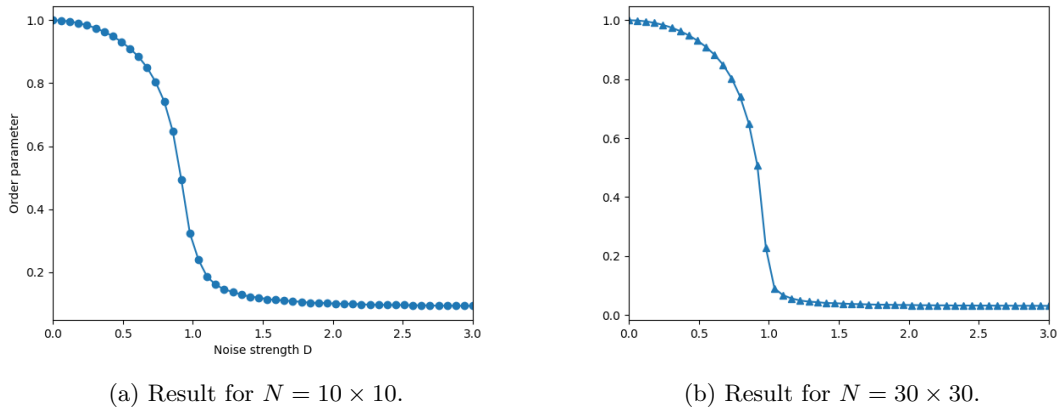


Figure 2.1: Variations of the order parameter due to changing noise strength for a system of N oscillators.

2.2.2 Milstein

The Euler-Forward method however is quite simple, and is of low order. An improvement on this is the Milstein method. This method also gives a strong approximation, but is of order 1. It is often used for its improved order over the Euler-Forward method, while still being relatively simple to implement. We can apply this method to the SDE

$$\dot{x}(t) = f(x) + \sigma(x)\dot{W}(t).$$

In the case of the Kuramoto model we have $f(x) = \left(\sum_j K_{ij} \sin(x_j - x_i) \right)_i^T$, where x_j denotes the j -th component of the random vector x , so θ_j in notation used earlier, and $\sigma(x) = D$.

The Milstein method is then defined as follows [6]:

$$x[t + \Delta t] = x[t] + f(x[t]) \cdot \Delta t + \sigma(x[t]) \cdot \Delta W[t] + \frac{1}{2} \sigma(x[t]) \sigma'(x[t]) (\Delta W[t]^2 - \Delta t).$$

Where $\Delta W[t]$ signifies the discretized derivative of the Wiener process as before, so $\Delta W[t] \sim \Delta t \cdot \mathcal{N}(0, 1)$.

While the term seems rather long, implementing this method is simple when $\sigma(x)$ is known. What makes it even easier in the case of the Kuramoto model, is the fact that the diffusion coefficient, $\sigma(x)$ that is, is constant. Thus, $\sigma' = 0$ and the Milstein method coincides with Euler-Forward.

2.2.3 On higher order methods

Higher order methods exist, but they were not used in this work. However, it seems fitting to at least mention them as a point for future improvement. The Milstein method can be expanded further to obtain the order $\frac{3}{2}$ strong Taylor scheme. The implementation of this however is rather complicated and requires the creation of new random variables.

A more suitable approach for the Kuramoto model is the Stochastic-Runge-Kutta- $\frac{3}{2}$ method. The method is still quite complicated to implement, for details see [5], but offers a method developed especially for SDEs with a constant diffusion coefficient (called scalar noise in [5]). An advantage of a Runge-Kutta like method is the absence of derivatives of f (and possibly σ , but these are zero for a constant diffusion coefficient) in the scheme, which allows for a more *plug-and-play* implementation.

3. Theory

In this chapter we will review some of the theoretical background provided in literature, as well as expand on this with further analysis. We will produce figures through own simulations [4], with the exception of one, which will be mentioned.

3.1 Kuramoto's analysis

The governing equation for a system of oscillators in the standard Kuramoto model is

$$\frac{d\theta_i}{dt} = \omega_i + \sum_j K_{ij} \sin(\theta_j - \theta_i). \quad (3.1)$$

Here each ω_i represents the natural frequency of the i -th oscillator, and K_{ij} indicates the coupling strength between oscillators i and j .

The ω_i are distributed according to some probability density. If we let $\Omega = \mathbb{E}[\omega]$ and transform our system to a rotating system, $\theta \rightarrow \theta - \Omega t$ that is, we can treat ω as a distribution with mean zero.

Kuramoto provided some analysis on the model in the case of infinitely many oscillators under mean field coupling. Below we work out the details in ref. [7].

We first define a phase locked solution as a solution in which $\dot{\theta}_i = \dot{\theta}_j$ where i and j are coupled oscillators.

Mean field coupling In Kuramoto's original analysis he considered the case of mean-field coupling. This is a means taking $K_{ij} = K/N > 0$ in equation 3.1. Using this method we can greatly simplify the Kuramoto model using what is called the order parameter

$$r e^{i\psi} = \frac{1}{N} \sum_j e^{i\theta_j}, \quad (3.2)$$

where r indicates the coherence and ψ is the mean phase. If we then look at $r e^{i(\psi - \theta_i)}$ we see that its imaginary part occurs in equation 3.1. Thus, we can simplify that equation to

$$\frac{d\theta_i}{dt} = \omega_i + K r \sin(\psi - \theta_i). \quad (3.3)$$

In the limit of infinitely many oscillators we may rewrite 3.2 into an integral with a new probability density $\rho(\theta, t | \omega)$ to obtain

$$r e^{i\psi} = \int_{-\pi}^{\pi} \int_{-\infty}^{\infty} e^{i\theta} \rho(\theta, t | \omega) g(\omega) d\omega d\theta. \quad (3.4)$$

Here $g(\omega)$ signifies the probability density of the eigen-frequencies ω in the system, which will take to be Gaussian for the rest of this thesis. The new density of phase $\rho(\theta, t | \omega)$ changes with θ and time, but it is subject to the given distribution of the eigenfrequencies.

Continuity condition The continuity condition for the density of phase can be derived with the argument stating that the number of states must be conserved. To this end, we consider a small fraction of $(-\pi, \pi]$, $\Delta\theta$, over a small amount of time, Δt . We denote the velocity of the states with ν . Then by conservation of states:

$$\begin{aligned} \Delta\theta \left(\rho|_t^{t+\Delta t} + \mathcal{O}(\Delta t^2) \right) &= \Delta t \left(\rho\nu|_{\theta+\Delta\theta}^{\theta} + \mathcal{O}(\Delta\theta^2) \right) \\ \frac{\rho|_t^{t+\Delta t}}{\Delta t} + \mathcal{O}(\Delta t) &= \frac{\rho\nu|_{\theta+\Delta\theta}^{\theta}}{\Delta\theta} + \mathcal{O}(\Delta\theta) \end{aligned}$$

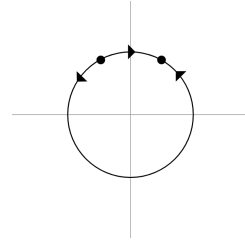
Then taking the limit $\Delta t \rightarrow 0$ and $\Delta\theta \rightarrow 0$ yields

$$\frac{\partial \rho}{\partial t} + \frac{\partial}{\partial \theta} (\rho\nu) = 0. \quad (3.5)$$

Stationary states for infinitely many oscillators We now consider infinitely many oscillators with eigenfrequencies ω and initial positions taken to be 0 w.l.o.g.¹ (without loss of generality) under mean field coupling. If we now look at equation 3.4 we can find $r = 0$ for a fully incoherent solution, or $r = 1$ for a fully synchronized solution. More interesting are partially synchronized solutions.

Suppose we take Ω to be the mean of all ω and transform the system along $\theta \rightarrow \theta - \Omega t$. We can see that a state is locked in phase with the mean, synchronized that is, whenever $\frac{d\theta}{dt} = 0$. Oscillators with $|\omega_i| < Kr$ can then become phase-locked with a phase difference with respect to the mean phase, being 0, which satisfies $\omega = Kr \sin(\theta)$. This yields the stable solution $\theta \in [-\pi/2, \pi/2]$ and unstable solution $\theta \in [\pi/2, 3\pi/2]$ as can be seen in figure 3.1. The latter has measure zero and does not have to be considered for the density. Thus, density for phase locking oscillators then becomes $\delta(\omega - Kr \sin(\theta))H(\cos(\theta))$, with H being the Heaviside function.

For the incoherent stationary states we note that $\frac{\partial \rho}{\partial t} = 0$, by stationarity. Thus from equation 3.5 we see that $\rho \nu$ is constant w.r.t. θ . We now write $\rho = C(\omega)/\nu$ to obtain an equation which does not depend on time explicitly. In the rotating frame chosen, we see that $\nu = \dot{\theta} = \omega + Kr \sin(\psi - \theta)$, something which Kuramoto saw intuitively [7]. Normalization of ρ then yields the distribution as given in equation 3.6 and shown in figure 3.2. The figure shows high density at $\pi/2$ and low density at $-\pi/2$ which is in accordance with the oscillators slowing down or speeding up respectively. For $\omega \rightarrow \infty$ the curves approach $1/2\pi$.



$$\rho = \begin{cases} \delta(\omega - Kr \sin(\theta))H(\cos(\theta)) & \text{for } |\omega| \leq Kr \\ \frac{\sqrt{\omega^2 - (Kr)^2}}{2\pi|\omega - Kr \sin(\theta_i)|} & \text{for } |\omega| > Kr \end{cases} \quad (3.6)$$

Figure 3.1: The stability of stationary states. ψ was chosen w.l.o.g. to be 0. The dots indicate the stationary points and the arrows indicate the direction in which a small deviation from a stationary point will travel.

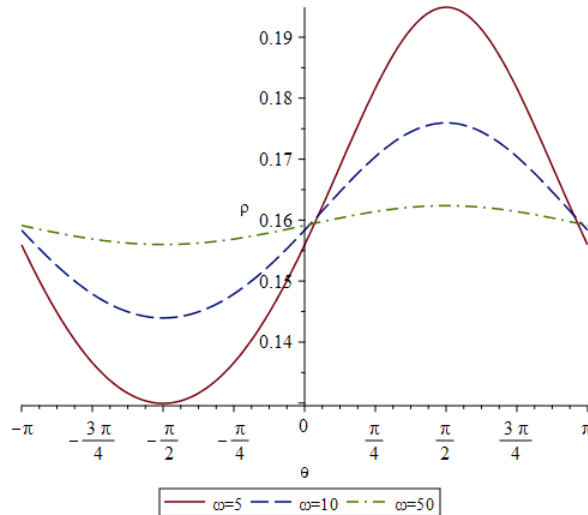


Figure 3.2: Plot of equation 3.6 for values of ω of 5, 10 and 50. Kr was taken as 1.

¹This can be done without loss of generality because the system only depends on phase differences between oscillators. If we add some arbitrary number Δ to each θ_i or θ we would result with $\dots \sin(\theta_j + \Delta - \theta_i - \Delta)$ or $\dots \sin(\psi + \Delta - \theta - \Delta)$.

Using the assumption that $g(\omega)$ is Gaussian allows us to combine and simplify equations 3.6 and 3.4. We will first note that the imaginary parts must vanish, as we have taken $\psi = 0$ w.l.o.g. We then split the integral in equation 3.4 over $|\omega| \leq Kr$ and $|\omega| > Kr$.

$$r = \int_{-\pi}^{\pi} \int_{|\omega| \leq Kr} \cos(\theta) \rho(\theta, t | \omega) g(\omega) d\omega d\theta + \int_{-\pi}^{\pi} \int_{|\omega| > Kr} \cos(\theta) \rho(\theta, t | \omega) g(\omega) d\omega d\theta.$$

We can now note that $\rho(\theta + \pi, t | -\omega) g(-\omega) = \rho(\theta, t | \omega) g(\omega)$ to evaluate that the second integral is zero.

$$\begin{aligned} \int_{-\pi}^{\pi} \int_{-\infty}^{-Kr} \cos(\theta) \rho(\theta, t | \omega) g(\omega) d\omega d\theta &= \int_{-\pi}^{\pi} \int_{-\infty}^{-Kr} \cos(\theta) \rho(\theta + \pi, t | -\tilde{\omega}) g(-\tilde{\omega}) d\tilde{\omega} d\theta \\ &= \int_{-\pi}^{\pi} \int_{Kr}^{\infty} \cos(\theta) \rho(\theta + \pi, t | \tilde{\omega}) g(\tilde{\omega}) d\tilde{\omega} d\theta \\ &= \int_0^{2\pi} \int_{Kr}^{\infty} \cos(\tilde{\theta} - \pi) \rho(\tilde{\theta}, t | \tilde{\omega}) g(\tilde{\omega}) d\tilde{\omega} d\tilde{\theta} \\ &= - \int_0^{2\pi} \int_{Kr}^{\infty} \cos(\tilde{\theta}) \rho(\tilde{\theta}, t | \tilde{\omega}) g(\tilde{\omega}) d\tilde{\omega} d\tilde{\theta} \\ &= - \left(\int_0^{\pi} \int_{Kr}^{\infty} \cos(\tilde{\theta}) \rho(\tilde{\theta}, t | \tilde{\omega}) g(\tilde{\omega}) d\tilde{\omega} d\tilde{\theta} \right. \\ &\quad \left. + \int_{\pi}^{2\pi} \int_{Kr}^{\infty} \cos(\tilde{\theta}) \rho(\tilde{\theta}, t | \tilde{\omega}) g(\tilde{\omega}) d\tilde{\omega} d\tilde{\theta} \right) \\ &= - \left(\int_0^{\pi} \int_{Kr}^{\infty} \cos(\tilde{\theta}) \rho(\tilde{\theta}, t | \tilde{\omega}) g(\tilde{\omega}) d\tilde{\omega} d\tilde{\theta} \right. \\ &\quad \left. + \int_{-\pi}^0 \int_{Kr}^{\infty} \cos(\tilde{\theta}) \rho(\tilde{\theta}, t | \tilde{\omega}) g(\tilde{\omega}) d\tilde{\omega} d\tilde{\theta} \right) \\ &= - \int_{-\pi}^{\pi} \int_{Kr}^{\infty} \cos(\tilde{\theta}) \rho(\tilde{\theta}, t | \tilde{\omega}) g(\tilde{\omega}) d\tilde{\omega} d\tilde{\theta} \end{aligned}$$

Thus, we are left with only the part for $|\omega| < Kr$, which we can easily integrate out because of the delta functions. From this we obtain

$$r = rK \int_{-\pi/2}^{\pi/2} \cos^2(\theta) g(Kr \sin(\theta)) d\theta. \quad (3.7)$$

This equation has a trivial solution $r = 0$ which corresponds to a fully incoherent solution, $\rho = 1/2\pi$ that is. It also has a separate branch

$$1 = K \int_{-\pi/2}^{\pi/2} \cos^2(\theta) g(Kr \sin(\theta)) d\theta. \quad (3.8)$$

This equation also has a solution for $r = 0$, which can be found easily by substituting $r = 0$ in g . This yields the critical coupling constant $K_c = \frac{2}{g(0)\pi}$, below which synchronization is not possible.

3.2 Phase transition for annealed noise

The physical systems modelled by the Kuramoto model are often subject to noise, for example in the form of thermal energy. In this section we will analyse the effect of noise of this form of noise, called annealed noise. For this our system will be a 2D torus of some size $N \times N$. As such, we now expand the Kuramoto model with a stochastic noise term $D\eta_i(t)$, which we will take to be Gaussian for the rest of this work. Also we leave out the individual ω_i . The constant D signifies the strength of the noise, $\eta_i(t)$ is the standard white noise added to the system. Furthermore we restrict ourselves to nearest-neighbour coupling, signified by the nn_i . The coupling strength usually denoted by K is left out through rescaling in time.

$$\frac{d\theta_i}{dt} = \sum_{j \in nn_i} \sin(\theta_j - \theta_i) + D\eta_i(t) \quad (3.9)$$

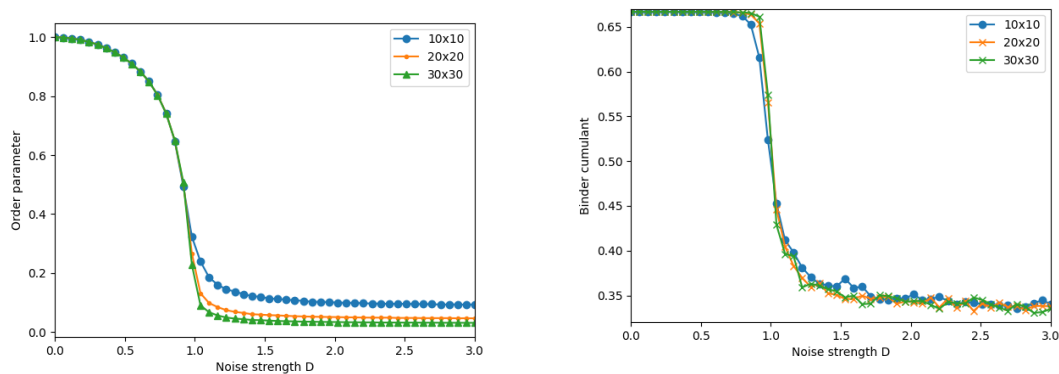
In figure 3.3 we show the simulated behaviour of the order parameter and Binder cumulant for varying noise strength D . The simulations were run using a self written Python script. These figures indicate a possible phase transition with some critical noise strength D_c . The (fourth order) Binder cumulant is defined by

$$U_r = 1 - \left[\frac{\langle r^4 \rangle}{3\langle r^2 \rangle^2} \right]. \quad (3.10)$$

Here $[\cdot]$ means taking a sample average and $\langle \cdot \rangle$ a time average in the steady state. We can then easily see that in the fully synchronized case $U_r = 2/3$, as r just takes the value 1 without fluctuation. Hence $\langle r^4 \rangle = 1 = \langle r^2 \rangle^2$ and thus $U_r = 2/3$.

The de-synchronized limit is a bit harder to see, as U_r does not approach 0 for increasing system size, which it is when applied to the Ising model [8]. In the case of the Kuramoto (or XY) model some articles directly claim it will approach 1/3 [9, 10], which it does, but these articles lack proof. We worked out a proof which can be found in the Appendix for the interested reader .

This Binder cumulant features a much sharper 'knee' and can be used for spotting where the phase-transition starts, which defines the critical D_c .



(a) The order parameter for a 10×10 , 20×20 and 30×30 system.

(b) The Binder cumulant for a 10×10 , 20×20 and 30×30 system. The drop curves off sharply at $D \approx 1$, indicating a phase transition at this point.

Figure 3.3: Simulation results of varying system sizes showing the order parameter and Binder cumulant depending on annealed noise strength.

For further estimation of D_c we look at a scaled variance of the order parameter for an $L \times L$ system, called the fluctuation, defined by

$$\chi_r(D, L) = L^d [\langle r^2 \rangle - \langle r \rangle^2]. \quad (3.11)$$

Here $[\cdot]$ and $\langle \cdot \rangle$ denote the same as before. The maximum of χ would then be at the point where the variation would be the largest. We can intuitively explain why this is. For $D < D_c$, synchronization will occur, thus we have an order parameter very close to 1 all the time. For $D > D_c$, synchronization is not possible. Hence the order parameter will consistently be relatively low. Only near the critical strength will we see jumps between synchronization and incoherence, so naturally the fluctuation will be the greatest at this point.

3.3 Synchronization phenomena for quenched noise

Now we will look at a simplification of 3.1, where we still take $K = 1$ w.l.o.g. Further we use nearest neighbour coupling as in the previous section.

$$\frac{d\theta_i}{dt} = \omega_i + K \sum_{j \in nn_i} \sin(\theta_j - \theta_i) \quad (3.12)$$

Here we assume that $\omega_i \sim \mathcal{N}(0, \sigma^2)$ i.i.d.

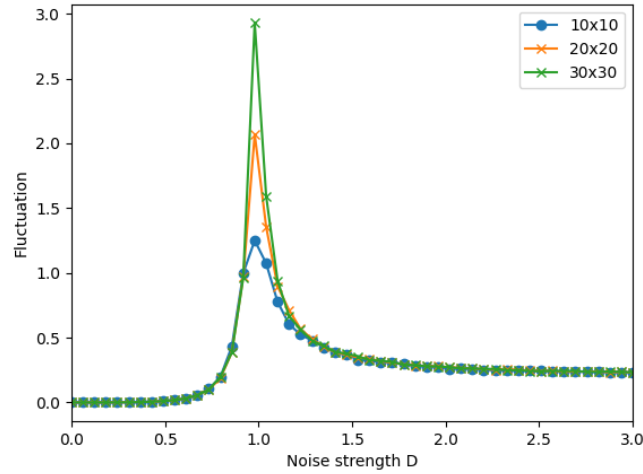
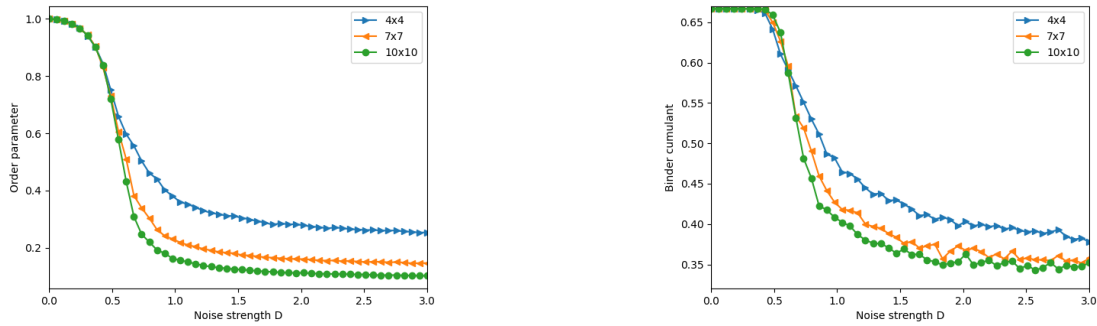


Figure 3.4: The simulated fluctuation for systems of varying sizes. Note that like in figure 3.3, the critical noise strength seems to be approximately 1.



(a) The order parameter for different, smaller system sizes. We now see some separation.

(b) The Binder cumulant for systems of different and smaller sizes, with quenched noise only.

Figure 3.5: The results of simulations for varying system sizes with quenched noise for a timespan of two minutes in the rescaled time.

It seems logical that for larger σ the model would have more trouble synchronizing. To investigate this plot of the order parameter and Binder cumulant are made and shown in figure 3.5.

For increasing system sizes an earlier drop-off in the Binder cumulant can be seen. An interesting result is that the order parameter has already decreased significantly when the Binder cumulant is just starting to decrease. This is due to what is called entrainment.

As we saw before in the mean field analysis, states can be stationary whenever $\omega_i = Kr \sin(\theta_i)$ after rotating the system to the mean phase. Thus, when increasing σ from 0, states can be locked in phase without bunching up into a singular point. This can be seen in the decrease of the order parameter.

At some point the order parameter has decreased so much that there no longer are solutions to $\omega_i = Kr \sin(\theta_i)$ for at least some oscillators. This happens at the critical quenched noise strength σ_c and is more accurately shown using the Binder cumulant in figure 3.5b.

3.3.1 Stability analysis

For the system with quenched noise only there is a nifty method for finding the critical quenched noise strength σ_c . This method is a physicist's second-favorite tool, with separation of variables being the first; perturbation theory.

Suppose we have some stationary state with phases θ . We will next apply a small perturbation to it which we will call $\delta\theta$. We take the perturbation sufficiently small to apply a linear approximation so that we find

$$\delta\dot{\theta} = \mathbf{J}(\theta, \omega)\delta\theta,$$

where \mathbf{J} is the Jacobian matrix evaluated at (θ, ω) . The elements of the Jacobian matrix are given by

$$\mathbf{J}_{ijkl} = \left. \frac{\partial}{\partial \theta_{kl}} F(\theta_{ij}, \theta_{kl}) \right|_{\theta}.$$

Here $F(\theta_{ij}, \theta_{kl}) = \omega_i + K \sum_{kl \in nn_{ij}} \sin(\theta_{kl} - \theta_{ij})$ which allows us to explicitly write out the Jacobian matrix.

The quadruple subscripts follow directly from the 2D model, with θ_{ij} denoting the oscillator at position (i, j) .

The entire Jacobian matrix would take up a lot of paper so it will be omitted here, but it can be seen in ref. [9] on p. 18 for the keen reader. An interesting property can be deduced without writing down the closed form.

We can note that the matrix is symmetric following from the evenness of the cosine. This implies that the eigenvalues are real, which simplifies stability analysis, where we can look at the eigenvalues to form a conclusion on stability.

We should note that the system is invariant under rotational translation as we explained before. A zero eigenvalue is always present because of this. Thus, we are interested in whether the largest eigenvalue is larger than 0.

The point at which the system starts to destabilize is marked by the appearance of an eigenvalue greater than 0. The perturbation for $\sigma \geq \sigma_c$ pushes some synchronized oscillators into another state, making the previous state unstable. This in turn causes a positive eigenvalue(s) to appear. Due to limits in computation time we show a figure of this made in ref. [9] in figure 3.6.

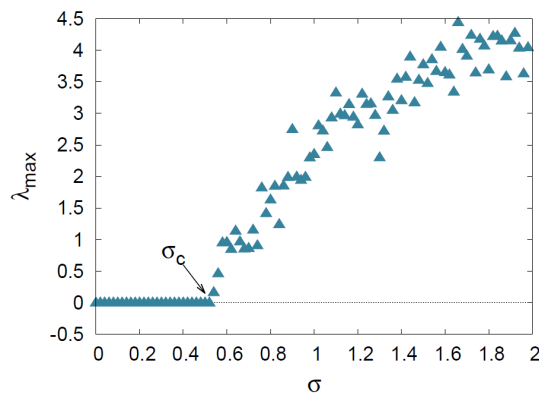


Figure 3.6: The result of simulations with the eigenvalue analysis taken from ref. [9].

3.3.2 Fractional synchronization

Suppose now that we are interested in the relation between the order parameter and the fraction of oscillators which are synchronized. We will denote this fraction f . This will be investigated under the assumption that the eigenfrequencies are drawn from a $\mathcal{N}(0, \sigma^2)$ distribution. This is then equivalent to stating that

$$f \approx \mathbb{P}(|\omega| < Kr) = \int_{-Kr}^{Kr} \frac{e^{-\frac{x^2}{2\sigma^2}}}{\sqrt{2\pi\sigma^2}} dx = \operatorname{erf}\left(\frac{Kr}{\sigma\sqrt{2}}\right), \quad (3.13)$$

where the approximation becomes increasingly accurate for increasing system sizes as a consequence of the law of large numbers.

We then look at equation 3.8 and simply substitute $u = Kr \sin(\theta)$ once again using the assumption that g is Gaussian to arrive at an integral equation quite like 3.13.

$$r = \int_{-Kr}^{Kr} \sqrt{1 - \frac{u^2}{(Kr)^2}} \frac{e^{-\frac{u^2}{2\sigma^2}}}{\sqrt{2\pi\sigma^2}} du$$

Now we note that we can use the extended binomial theorem to expand the square root in terms of even powers of u ;

$$\sqrt{1 - \frac{u^2}{(Kr)^2}} = \sum_{i=0}^{\infty} \binom{1/2}{i} \left(\frac{-1}{(Kr)^2} \right)^i u^{2i}. \quad (3.14)$$

We can then use induction to relate integrals as such:

$$\int_{-Kr}^{Kr} u^{2n} \frac{e^{-\frac{u^2}{2\sigma^2}}}{\sqrt{2\pi\sigma^2}} du = (2n-1)\sigma^2 \int_{-Kr}^{Kr} u^{2(n-1)} \frac{e^{-\frac{u^2}{2\sigma^2}}}{\sqrt{2\pi\sigma^2}} du - \sigma^2 \frac{(Kr)^{2n-1} \sqrt{2} e^{-\frac{(Kr)^2}{2\sigma^2}}}{\sqrt{\pi\sigma^2}}.$$

Putting this together into we find that

$$\begin{aligned} \int_{-Kr}^{Kr} x^{2n} \frac{e^{-\frac{x^2}{2\sigma^2}}}{\sqrt{2\pi\sigma^2}} du &= - \left(\sum_{i=0}^{n-1} \sigma^2 (Kr)^{2(n-i)-1} \sqrt{\frac{2}{\pi\sigma^2}} e^{-\frac{(Kr)^2}{2\sigma^2}} \frac{(2n-1)!! \sigma^{2i}}{(2(n-i)-1)!!} \right) + (2n-1)!! f \sigma^{2n} \\ &= I(n, \sigma, Kr, f). \end{aligned} \quad (3.15)$$

Here I is shorthand notation. We then then put this together with equation 3.14 to obtain that

$$r = \sum_{i=0}^{\infty} \binom{1/2}{i} \left(\frac{-1}{(Kr)^2} \right)^i I(i, \sigma, Kr, f). \quad (3.16)$$

Finally, we can eliminate Kr from this by using 3.13, such that $Kr = \sigma\sqrt{2}\text{erf}^{-1}(f)$:

$$r = \sum_{i=0}^{\infty} \binom{1/2}{i} \left(\frac{-1}{(\sigma\sqrt{2}\text{erf}^{-1}(f))^2} \right)^i I(i, \sigma, \sigma\sqrt{2}\text{erf}^{-1}(f), f). \quad (3.17)$$

However, using this last substitution will not yield better results than $f = \text{erf}\left(\frac{Kr}{\sigma\sqrt{2}}\right)$ itself will. Hence it might be more interesting to leave the result at equation 3.16, as it omits the error function. Using this result to approximate an implicit relation between f and r or σ/Kr seems difficult though, a lot of complicated math is needed to work out a few terms yielding only the result in figure 3.7.

A perhaps easier result is the relation we started with, namely $f = \text{erf}\left(\frac{Kr}{\sigma\sqrt{2}}\right)$, which yields the green line in figure 3.7. If we zoom in more by leaving out the result of 3.16 we see that this assumption was not unreasonable, but could be better, as can be seen in figure 3.8. The assumption and simulated values did become closer as the system size increased.

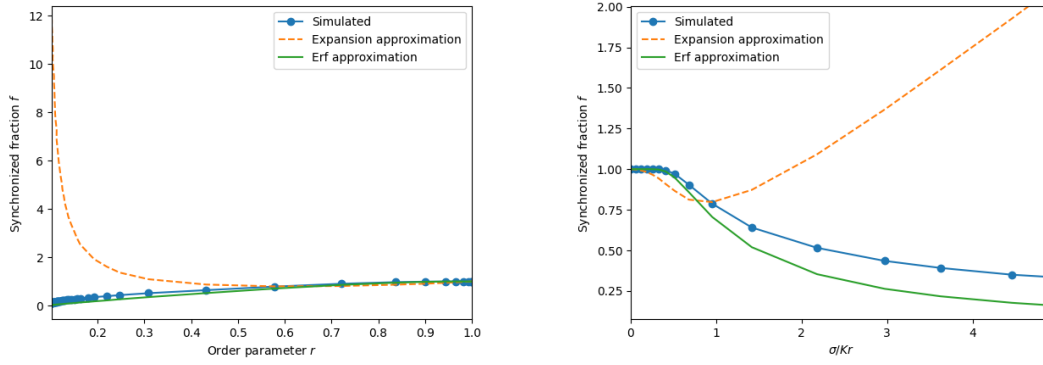


Figure 3.7: The result of a 10×10 simulation with noise strength ranging from 0 to 3. The solid green line represent the error-function assumption, the dashed orange line is the first two terms of eq 3.17.

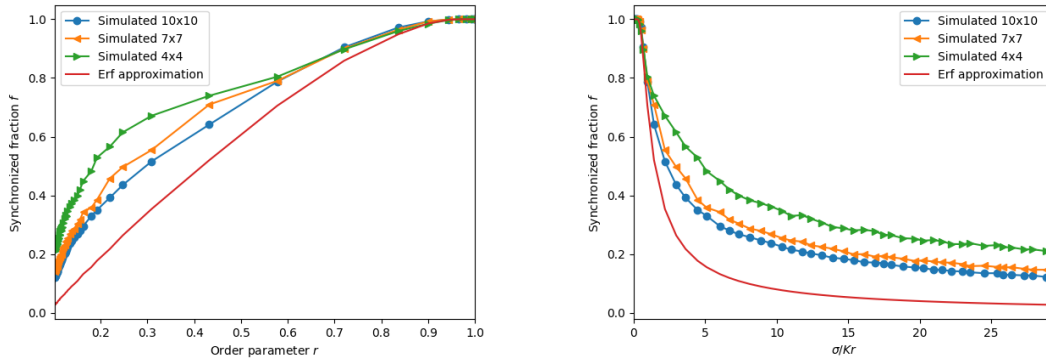


Figure 3.8: The result of simulations for varying system sizes with noise strength ranging from 0 to 3. The red line represents the initial assumption that $f = \operatorname{erf}\left(\frac{Kr}{\sigma\sqrt{2}}\right)$.

3.3.3 Synchronization requirements

We will now take a deeper dive into when synchronization is possible and stability. We will investigate this on rings and coupled rings.

1D nearest neighbor coupling

We consider a 1D case of nearest neighbor coupling with quenched noise only. We take N to be the number of oscillators. In this case we can look at two coupled oscillators and equate their Kuramoto equations (3.12) to find what is needed for phase locking. We then after eliminating θ_{i+1} through rotating the system obtain

$$|\omega_i - \omega_{i+1}| = K |2 \sin(\theta_i) + \sin(\theta_{i+2}) - \sin(\theta_{i-1})|.$$

Thus, we need

$$K \geq \frac{|\omega_i - \omega_{i+1}|}{4} \quad (3.18)$$

if we want synchronization with the mean $\frac{1}{N} \sum_{i=1}^N \omega_i$ of the system to be possible. In the case of three oscillators 4 is replaced by 2, as this case coincides with mean field coupling. If we assume the ω to be $\mathcal{N}(0, \sigma^2)$ i.i.d. we can find synchronization probabilities using the following

$$\begin{aligned} \mathbb{P}\left(16K^2 \underset{\geq}{\leq} (\omega_i - \omega_{i+1})^2\right) &= \mathbb{P}\left(16K^2 \underset{\geq}{\leq} \mathcal{N}^2(0, 2\sigma^2)\right) \\ &= \mathbb{P}\left(\frac{8K^2}{\sigma^2} \underset{\geq}{\leq} \mathcal{N}^2(0, 1)\right) \\ &= \mathbb{P}\left(\frac{8K^2}{\sigma^2} \underset{\geq}{\leq} \chi_1^2\right). \end{aligned}$$

We then have $N - 1$ independent differences in eigenfrequencies. The probability of partial synchronization being possible is then

$$1 - \mathbb{P} \left(\chi_1^2 \geq \frac{8K^2}{\sigma^2} \right)^{N-1} \quad (3.19)$$

and the probability of total synchronization being possible is

$$\mathbb{P} \left(\chi_1^2 \leq \frac{8K^2}{\sigma^2} \right)^{N-1}. \quad (3.20)$$

This is a result somewhat similar to that of found by Strogatz and Mirollo [11].

Suppose now we add some annealed noise $\eta_i(t)$ for each oscillator with a $\mathcal{N}(0, D^2)$ distribution. When doing this it becomes important to ask what we define to a synchronized state to be, as a small fluctuation will always be present. The figures in the next section were generated using a histogram of oscillator velocities (θ s). A solution was taken to be fully synchronised if all velocities were in the same bin, and partially synchronised if any bin has height greater than $1/N$. Depending on the bin sizes this might be a valid method. For the verification in this work we used a bin size of $4\sqrt{\sigma^2 + D^2}/11$.

We can then do the same analysis as before, with $\omega_i - \omega_{i+1} + \eta_i(t) - \eta_{i+1}(t) \sim \mathcal{N}(0, 2(\sigma^2 + D^2))$. We can then easily write out the probability of partial synchronization being possible as

$$1 - \mathbb{P} \left(\chi_1^2 \geq \frac{8K^2}{\sigma^2 + D^2} \right)^{N-1} \quad (3.21)$$

and the probability of total synchronization being

$$\mathbb{P} \left(\chi_1^2 \leq \frac{8K^2}{\sigma^2 + D^2} \right)^{N-1}. \quad (3.22)$$

We can then see that both situations are less likely.

Three oscillators

In the special case of three oscillators without annealed noise we already saw that the factor 4 does not hold, but more can be said in the case of total synchronization. We thus fill in $N = 3$ in equations 3.22 and 3.21 to obtain the partial synchronization probability

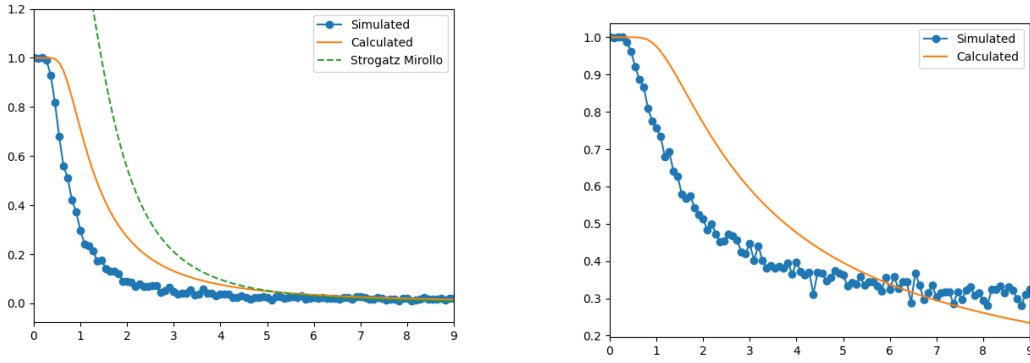
$$1 - \mathbb{P} \left(\chi_1^2 \geq \frac{2K^2}{\sigma^2 + D^2} \right)^2$$

and total synchronization probability

$$\mathbb{P} \left(\chi_1^2 \leq \frac{2K^2}{\sigma^2 + D^2} \right)^2.$$

First, we introduce simulation results of these probabilities, given in figure 3.9. The results with annealed noise are given in figure 3.10.

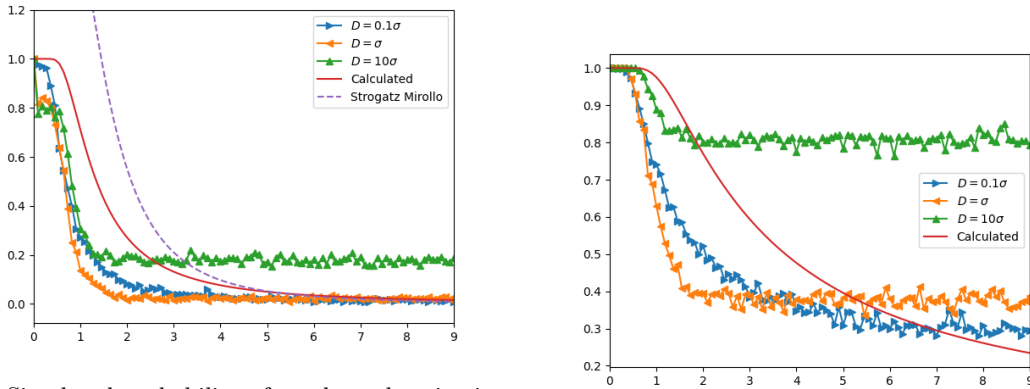
Here we see some interesting behaviour in figure 3.10. The curves seems to drop off significantly lower for noise strength < 2 . Figure 3.10b however also shows the problem with the histogram method and defining synchronization in a stochastic sense. A lower limit greater than 0 seems to be reached which is due to the annealed noise interfering with the histogram method.



(a) Simulated probability of total synchronization for a system of 3 oscillators. Both the bound by Strogatz and Mirollo and the calculation in this work are shown.

(b) Simulated probability of partial synchronization for a system of 3 oscillators, with a calculated upper bound

Figure 3.9: Simulation results of synchronization probabilities for a system of 3 oscillators with quenched noise.



(a) Simulated probability of total synchronization for a system of 3 oscillators including annealed noise in different ratios to the quenched noise, with a calculated upper bounds. Both the bound by Strogatz and Mirollo and the calculation in this work are shown.

(b) Simulated probability of partial synchronization for a system of 3 oscillators including annealed noise, with a calculated upper bound

Figure 3.10: Simulation results of synchronization probabilities for a system of 3 oscillators including annealed noise.

Stability of the 3-ring solutions We now take a step back to the case where $D = 0$. For any fully-synchronized solution to be stable, the eigenvalues need to be 0, which will always be present due to the rotational invariance, and less than 0. For a system this small and simple we can analytically work out what was done in section 3.3.1. We can then find that the two non-zero eigenvalues are given by

$$\lambda_{1,2} = K \left[\begin{aligned} & -\cos(\theta_1 - \theta_3) - \cos(\theta_2 - \theta_3) - \cos(\theta_1 - \theta_2) \\ & \pm \left((\cos(\theta_1 - \theta_3) + \cos(\theta_2 - \theta_3) + \cos(\theta_1 - \theta_2))^2 \right. \\ & \left. - 3(\cos(\theta_1 - \theta_2)\cos(\theta_1 - \theta_3) + \cos(\theta_1 - \theta_2)\cos(\theta_2 - \theta_3) + \cos(\theta_1 - \theta_3)\cos(\theta_2 - \theta_3)) \right)^{1/2} \end{aligned} \right].$$

We note that the term in front of the square root is also squared within it. This means that we can only have both eigenvalues negative if this term is negative and also

$$\cos(\theta_1 - \theta_2) \cos(\theta_1 - \theta_3) + \cos(\theta_1 - \theta_2) \cos(\theta_2 - \theta_3) + \cos(\theta_1 - \theta_3) \cos(\theta_2 - \theta_3) \geq 0.$$

We can utilize the zero eigenvalue corresponding to rotational invariance to remove θ_3 , so

$$\cos(\theta_1 - \theta_2) \cos(\theta_1) + \cos(\theta_1 - \theta_2) \cos(\theta_2) + \cos(\theta_1) \cos(\theta_2) \geq 0.$$

We can then impose phase-locking to find the following conditions to be met by any solution,

$$\begin{aligned} \frac{\omega_3 + \omega_2}{K} &= \sin(\theta_2 - \theta_1) - \sin(\theta_1) \\ \frac{\omega_3 + \omega_1}{K} &= \sin(\theta_1 - \theta_2) - \sin(\theta_2). \end{aligned}$$

A visual representation of this is given in figures 3.11 and 3.12 in the form of level curves. The curves in figure 3.11a correspond to particular values of $(\omega_2 + \omega_3)/K$, whereas the curves in figure 3.11b correspond to values of $(\omega_1 + \omega_2)/K$. The intersections of curves in figure 3.11a and 3.11b thus define the possible synchronized solutions for some set of values $\{\omega_1, \omega_2, \omega_3, K\}$. The fact that any solution must lie on these level curves yields a nice visual representation of entrainment.

From these figures we see that for any set of values $\{\omega_1, \omega_2, \omega_3, K\}$ there are two at most possible synchronized solutions, but combining this with figure 3.11c leaves us with the only stable solution, of which there can be at most one.

We will elaborate a bit more on figure 3.11c. One might expect that solutions would only be stable in the region $[-\pi/2, \pi/2]^2$, yet we observe a different region. This is simply because of the origin not representing the mean phase, but one of the three oscillators' phase.

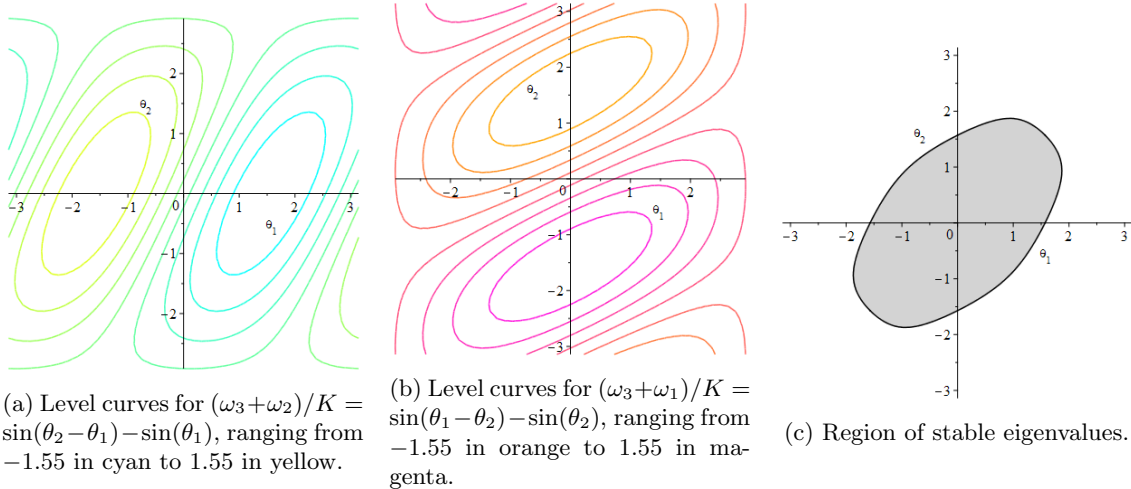


Figure 3.11: Stable region and level curves for the phase-locking conditions.

Table 3.1: Phase differences of the system as given in figure 3.13. Here $\delta_i = \omega_i - \Omega$, with Ω being the mean frequency of the system. We omit the $\pi - \arcsin$ solutions since they are not stable.

Phases	Difference
$\theta_6 - \theta_5$	$\arcsin(p + \delta_6/K)$
$\theta_5 - \theta_4$	$\arcsin(p + (\delta_6 + \delta_5)/K)$
$\theta_4 - \theta_6$	$\arcsin(p)$
$\theta_4 - \theta_3$	$\arcsin((\delta_4 + \delta_5 + \delta_6)/K)$ $\arcsin(-(\delta_1 + \delta_2 + \delta_3)/K)$
$\theta_3 - \theta_2$	$\arcsin(q - (\delta_1 + \delta_2)/K)$
$\theta_2 - \theta_1$	$\arcsin(q - \delta_1/K)$
$\theta_1 - \theta_3$	$\arcsin(q)$

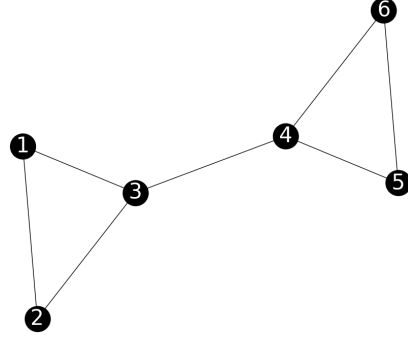


Figure 3.13: The system of two coupled 3-rings used.

Now we note that the difference $\theta_4 - \theta_3$ has two solutions, which must thus be equal in order to achieve synchronization, yielding that

$$\frac{\sum_{i=1}^6 \delta_i}{K} = 0$$

must be true. This is always the case by how the δ_i were defined, by taking $\delta_i = \omega_i - \Omega$ that is. This implies that stability of the coupled system depends on the stability of the individual rings and $(\delta_4 + \delta_5 + \delta_6)/K^2$ being in $(-1, 1]$ independently, not through some complicated relation.

Now as in [12], we need to have that the sum of all differences in a ring must equal a multiple of 2π , as it must of course make an integer amount of circles. Here we have a choice to make on how we take the arc-sines, so we either choose our branch in $(-\pi/2, \pi/2]$ or in $(\pi/2, 3\pi/2]$. This choice could be different for each phase difference, but if we want stable solutions only one branch is allowed. Solutions of a ring are stable if and only if the phase-differences lie in $(-\pi/2, \pi/2]$ [13]³. As such, this is how we choose our branches.

Knowing this it is possible to calculate a limit on the amount of stable solutions in systems consisting of arbitrary ring sizes. For a ring with N oscillators we have solutions for N phase differences in $(-\pi/2, \pi/2]$, of which the sum must be a multiple of 2π . Thus the maximal total phase difference we can achieve is $\pm N\pi/2 = 2m\pi$, so we see that m can take values in $-\lfloor N/4 \rfloor, \dots, 0, \dots, \lfloor N/4 \rfloor$. This m is also called the winding number, as it indicates how many full turns (or windings) the solution makes. The total phase difference for each ring, denoted by Φ below, can easily be generalised as such:

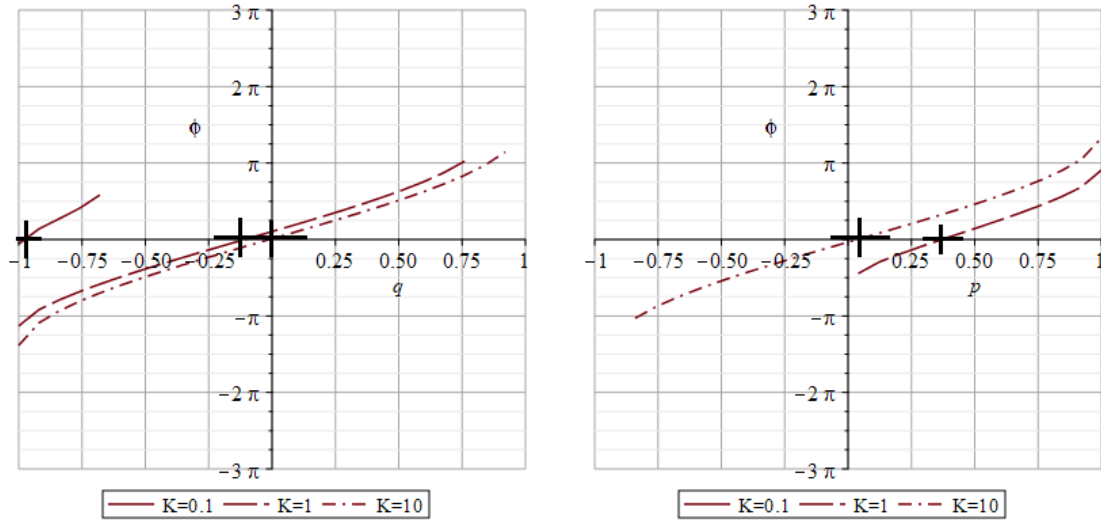
$$\text{Left: } \Phi_L = \sum_{i=0}^{N_{\text{left}}-1} \arcsin\left(q - \frac{1}{K} \sum_{j=1}^i \delta_j\right), \text{ right: } \Phi_R = \sum_{i=0}^{N_{\text{right}}-1} \arcsin\left(p + \frac{1}{K} \sum_{j=1}^i \delta_{N_{\text{total}}+1-j}\right).$$

We now have at most $2\lfloor N/4 \rfloor + 1$ winding numbers per ring. We can then invoke injectivity of the arc-sine to realise that this is also the amount of stable solutions. From the windings numbers we can solve for p or q s.t $\Phi_L = 2m_1\pi$ or $\Phi_R = 2m_2\pi$ respectively. Thus, for a system consisting of two coupled rings of sizes N_1 and N_2 we have at most $(2\lfloor N_1/4 \rfloor + 1) \times (2\lfloor N_2/4 \rfloor + 1)$ stable solutions, depending on the coupling constant K .

For a $3 + 3$ system this equates to one single stable solution, with the winding number for both rings being 0. This is shown in figure 3.14. The figure shows Φ_L and Φ_R for all values of q and p and the stable solutions lie at the points where the line has height $2m\pi$. A demonstration for a ring consisting of 7 oscillators is shown in figure 3.15. This figure shows three stable solutions for $K = 10$, which coincides with $2\lfloor 7/4 \rfloor + 1 = 3$.

²Or $\arcsin(-(\delta_1 + \delta_2 + \delta_3)/K)$.

³Dankjewel Johan :)



(a) The left ring with $(\omega_1, \omega_2, \omega_3) = (-0.21, -0.05, -0.05)$. (b) The right ring with $(\omega_4, \omega_5, \omega_6) = (1.15, -1.05, -0.08)$.

Figure 3.14: The curves defined implicitly by taking the sum of phase differences in the rings of 3 oscillators to be equal to ϕ . The left ring admits solutions for $K = 0.1$ whereas the right ring does not. Note that the only intersection with $2m\pi$ is at $\phi = 0$, so there is only one stable solution. The stable solutions are marked with a \pm .

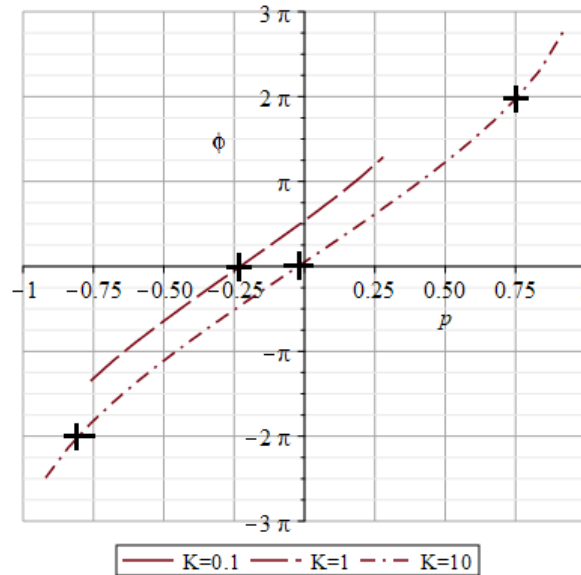


Figure 3.15: The curves defined implicitly by taking the sum of phase differences in the ring of 7 oscillators to be equal to ϕ . We see no solutions for $K = 0.1$, one for $K = 1$ and three for $K = 10$. The stable solutions are marked with a \pm .

4. Ising and XY model

4.1 Ising model

The Ising model describes the alignment of magnetic spin in a lattice. The spins cause a local magnetization, which makes it such that aligned spins are in a lower energy state, which is more favorable. This could cause materials to be magnetic, were it not for thermal excitations. Heat causes the spins to fluctuate, destroying alignment. For low temperatures however, this effect is small and we may see magnetization. This process can occur rapidly as a phase transition, which is called spontaneous magnetization.

In the Ising model each spin σ_i can take values 1 or -1 corresponding to spin *up* or spin *down*. The effect of neighbouring spins is then assumed to only be felt from nearest neighbours, so that we may write out the Hamiltonian of the system

$$H(\boldsymbol{\sigma}) = - \sum_{\langle ij \rangle} J_{ij} \sigma_i \sigma_j - \sum_i E \sigma_i. \quad (4.1)$$

In this equation $\langle ij \rangle$ denotes that i and j must be nearest neighbours, so it is equal to $\sum_i \sum_{j \in \text{nn}_i}$ in the notation used in the previous chapter. J_{ij} gives the interaction between spins i and j , which is usually taken to be independent of i, j . The quantity E denotes influence of an external magnetic field. The external field is often taken to be zero.

This model shows no phase transition in 1D, but it does in 2D, as was shown by Peierls in 1936.

4.2 XY model

We can generalize the previous Hamiltonian (eq 4.1) in the case of no external field for spins pointing in any direction instead of just up or down. Then we obtain

$$H(\boldsymbol{\sigma}) = - \sum_{\langle ij \rangle} J_{ij} \langle \boldsymbol{\sigma}_j \boldsymbol{\sigma}_i \rangle = - \sum_{\langle ij \rangle} J_{ij} \cos(\theta_j - \theta_i). \quad (4.2)$$

Here $\langle \boldsymbol{\sigma}_i \boldsymbol{\sigma}_j \rangle$ denotes the inner product of the spin vectors with length 1 of oscillators i and j , which equals the $\cos(\theta_j - \theta_i)$ we have already seen in equations 3.1, 3.9 and 3.12.

We can easily find the link between this and the Kuramoto model by realising that

$$\nabla H(\boldsymbol{\sigma}) = \left(\frac{d \left(- \sum_{j \in \text{nn}_i} J_{ij} \cos(\theta_j - \theta_i) \right)}{d\theta_i} \right)_{i \in \{1, \dots, N\}}^T \quad (4.3)$$

$$= \left(\sum_{j \in \text{nn}_i} J_{ij} \sin(\theta_j - \theta_i) \right)_{i \in \{1, \dots, N\}}^T = \frac{d\boldsymbol{\theta}}{dt} \quad (4.4)$$

is a case of the Kuramoto model without any form of noise. It is interesting to note that the gradient of the Hamiltonian results in a first derivative of its coordinates. This is called a gradient system.

4.2.1 The KT-transition

Now we will look at the Nobel-prize winning KT (Kosterlitz Thouless) transition. For this we will look at an $L \times L$ lattice of spins within the XY model with constant coupling $J_{ij} = J$. Then we approximate the cosine in the Hamiltonian up to the second order which, after neglecting constant energy, results in

$$H(\boldsymbol{\sigma}) = \frac{J}{2} \sum_{\langle ij \rangle} (\theta_j - \theta_i)^2.$$

This approximated system, called the spin-wave Hamiltonian, like the original, is invariant under a rotation of the entire system. This is called a continuous symmetry, because the system does not change when adjusting this continuous parameter. The Mermin-Wagner theorem then states that no ordinary phase-transition can occur [14, 15], because of the continuous symmetry in the system. The correlation function can be shown to be [16]

$$\langle e^{i(\theta(r)-\theta(0))} \rangle \sim r^{-k_b T/2\pi J}.$$

This indeed goes to zero as $r \rightarrow \infty$, so no long-range order can exist in the system. Yet, we still see a transition in the XY-model, which is due to vortices, which are not captured accurately in the spin-wave Hamiltonian.

A vortex is a set of four spins which, when travelling along them in a clockwise-manner, rotate clockwise. An anti-vortex rotates anti-clockwise when traversing clockwise. This is indicated in figure 4.1. A pair of vortices consists of a vortex and an anti-vortex.

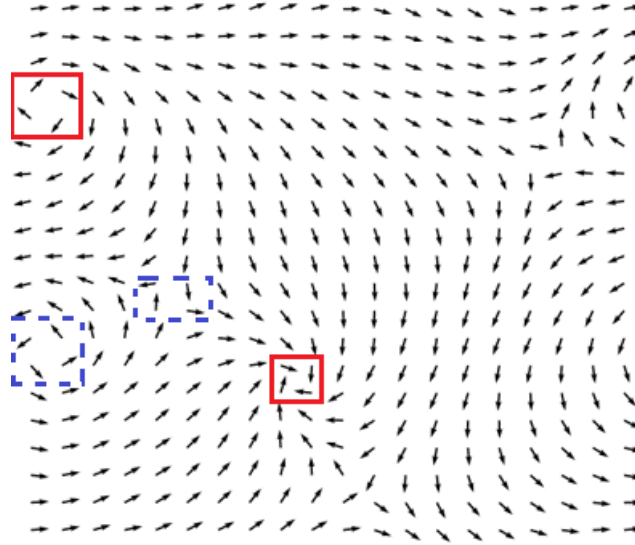


Figure 4.1: A simulated state of the XY-model at $T = 0$. A few obvious vortices (solid, red) and anti-vortices (dashed, blue) are outlined.

For the energy of such a vortex we look at the energy cost on a circle, with perimeter $2\pi r$ and thus $2\pi r/a$ spins on that perimeter. Here a is the lattice constant. The difference between two adjacent sites then is $2\pi \frac{a}{2\pi r} = \frac{a}{r}$, so we see that

$$E = \frac{2\pi J}{a^2} \int_a^L \frac{1}{2} \left(\frac{a}{r}\right)^2 r dr = J\pi \ln L/a.$$

Also we observe that the entropy of a vortex is $S = k_b \ln \Omega \approx k_b \ln \left(\frac{L}{a}\right)^2$. We can now write out the Helmholtz free energy of a vortex as

$$F = (\pi J - 2k_b T) \ln L/a.$$

Thus we observe that we cross $F = 0$ whenever

$$T = \frac{\pi J}{2k_b}.$$

We will denote this temperature by T_c , where c indicates it being the critical temperature. For T above this T_c negative free energy occurs for a single vortex, so it becomes energetically favorable to form free vortices. Below T_c the converse hold.

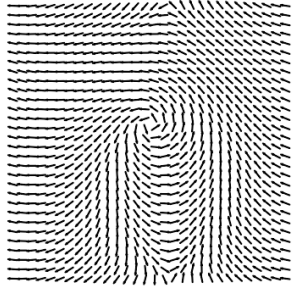
A pair of vortices however has energy independent of L , namely $E \sim J \ln(r/a)$ with r being the distance between the two vortices. The entropy of such a pair still scales with the logarithm of the system size, so we see that a pair of vortices may occur for $T < T_c$.

Kuramoto model

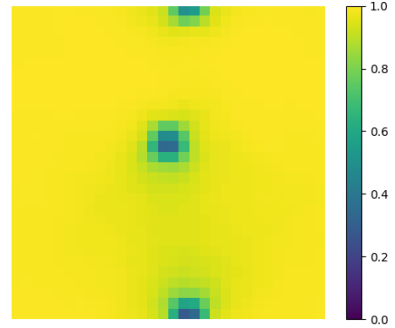
One may wonder then, would the more general quenched noise including of the Kuramoto model also show this behaviour? The answer to this is a yes. It has been shown in ref. [1] using figures for the case of no quenched noise, which we already discussed in the previous paragraph. It has more interestingly also been shown through a lengthy and complicated transformation of the partition functions of the XY and Kuramoto model for oscillators with differing eigenfrequencies. We can find these numerically and show them, as in figure 4.2.

A final question on the duality of these models then is on the annealed noise introduced in section 3.2. The simple answer is that this is hidden in the temperature. The annealed noise gives random 'kicks' according to some distribution which can be seen in the average velocity of the oscillators, which define the temperature of a solution.

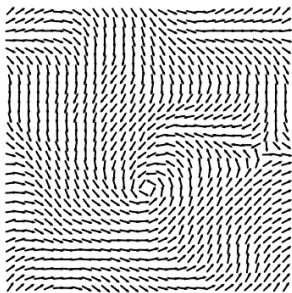
These two forms of noise then do not hinder the characteristics shown by the XY model, suggesting that the link between the XY and Kuramoto model is very strong.



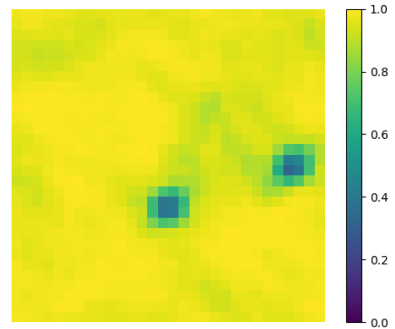
(a) Phases simulated with eigenfrequencies with variance 0.



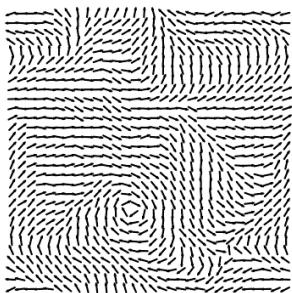
(b) Local order parameter simulated with eigenfrequencies with variance 0.



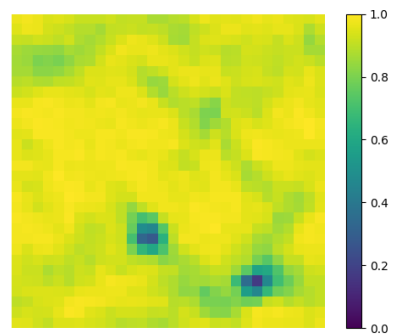
(c) Phases simulated with eigenfrequencies with variance 0.25.



(d) Local order parameter simulated with eigenfrequencies with variance 0.25.



(e) Phases simulated with eigenfrequencies with variance 0.45.



(f) Local order parameter simulated with eigenfrequencies with variance 0.45.

Figure 4.2: Simulation results for a Kuramoto model with nearest neighbour coupling and a system size of 30×30 .

5. Discussion

5.1 Analytical results

Most of the analytical results speak for themselves, but there are two for which some discussion is of interest.

Firstly we look back to section 3.3.2 on partial synchronization. The difference between the simulated values and the expansion approximation is large, the characteristics do not carry over well. The complicated result then in equation 3.16 yields little value, but does relate the synchronized fraction f and order parameter r without the error-function assumption on which it was based. Perhaps this could bring an expansion for the error-function.

The assumption itself gave a better approximation, which was approached by simulation results as the system size increased.

Secondly, we look at the synchronisation probability for a ring of three oscillators in section 3.3.3. The probability calculated in equations 3.19, 3.20 give rise to the same error-function like behaviour as in ref. [11], but with some different scaling factors. The probability calculated in section 3.3.3 seems to be much closer. The partial synchronization probability seemed to be off somewhat, this could be due to the histogram method problem which was more visible when including annealed noise.

Incorporating annealed noise complicated the result. The histogram method used seemed to fail when noise strengths increased above $D \approx 1$, visible especially from the large fluctuations and high probability in the high noise limit in figure 3.10b. Improving on this could perhaps be done by choosing a clever scaling of bin sizes in the histogram, or by using a more robust definition of phase-locking in the case of stochastic noise.

5.2 Numerical accuracy

When switching from deterministic problems to SDEs more is lost than just integration schemes. We also lose methods for estimating the error in the solution.

Luckily, our system shows the same dynamics in almost all situations. This allows us to find an *accurate enough* step size by inspection. Of course it should be noted that this *accurate enough* holds little quantifiable value, hence the inclusion of differences over step sizes shown below. Further, the figures produced in chapter 3 match the figures in ref. [9] at a step size of $\Delta t = 1/15$ in rescaled time. These facts provide confidence in the numerical accuracy of simulations ran.

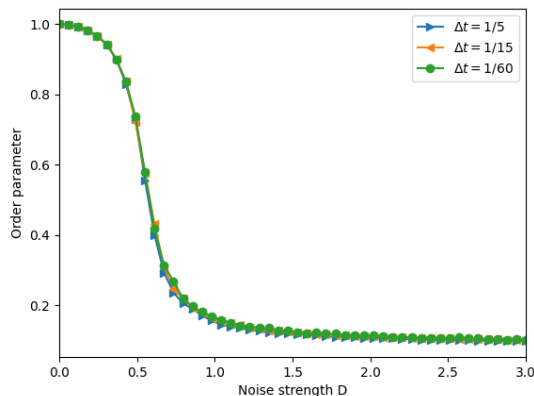


Figure 5.1: Simulation results of the order parameter on a 10×10 system with varying step sizes.

6. Conclusion

We elaborated on the methods of numerical analysis used for producing the results in this work. We started simple by listing some good practices when dealing with SDEs and then moved on to integrating methods for SDEs. These methods were of lower order than one may be used to when integrating deterministic differential equations, but fortunately the Kuramoto model allowed us to easily use a scheme of order 1. This was due to the diffusion coefficient being a constant, which caused the otherwise order 1/2 Euler-forward method to coincide with the order 1 Milstein method.

We also slightly touched on higher order methods for integrating SDEs. These methods do yield a higher order and implementation is possible for future improvement. In particular the Runge-Kutta method could deliver a *plug and play* experience once the code is written, providing good ease of implementation for further expansion of the model.

After this chapter we set out to understand and recreate the results in ref. [9]. This introduced notions of the Binder cumulant, fluctuation and an analysis of stability of stationary solutions. We also proved the result that in the de-synchronized limit of a mean field coupled system we have that the Binder cumulant approaches 1/3.

Section 3.3.2 then introduced an attempt to relate the fraction of oscillators which become synchronized to the order parameter. The expansion attempt did not show great results for the first few terms, but it did yield experience in working with the extended binomial theorem and expanding difficult terms. The assumption on which it was based gave a better approximation which was approached by simulation results as the system size increased.

Moving on then we attempted calculating a different quantity, namely the probability of either partial or total synchronization being possible. The resulting equations showed some similar behaviour to a result found by Strogatz and Mirollo [11]. The bound obtained however seemed to be more accurate, at least in the case of total synchronization of a ring consisting of three oscillators without annealed noise.

The addition of annealed noise caused some problems however. For low levels of noise strength ($D < 1$) the bound seemed to be accurate still. Above this we observed high probability in the high noise limit and large fluctuations. A better definition for synchronization seems needed to verify the results.

The stability analysis carried out after this yielded good results on the amount of stable solutions for a predefined system of three oscillators on a ring. The level curves gave a, in my eyes rather elegant, visual representation of entrainment. Intersecting these level curves yielded two points of which only one could lie in the region of stability, so we found only one possible stable solution. This is in accordance with the analysis carried out in the next section, noting that $2 \cdot \lfloor 3/4 \rfloor + 1 = 1$.

In the final section of chapter 3 we explored a coupling of two rings. We found an upper bound on the amount of stable solutions such a coupled system could have, which we showed by introducing the winding number. The stability of the entire system proved to be a simple combination of three parts; the stability of each individual ring and the possibility of the linking phase difference having a solution. We showed this in greater extent by introducing an independent coupling constant for each of these parts, which did not change stability of the overall system if the three parts were stable.

The final chapter took us to a more physics-centered look on the Kuramoto model. We researched literature of the Ising and XY model, the latter of which showed a clear link with the Kuramoto model. We then strengthened the link between the Kuramoto model and the XY model by showing that the inclusion of noise, be it quenched or annealed, does not break the duality. This was worked out extensively by transforming partition functions in ref. [1] and shown using figures in this work.

The stability analysis performed on the coupling of rings has applications specifically in electrical networks such as power grids. These grids however follow the second order Kuramoto model, which may alter some properties of the solutions found. This is a suggested point of future research.

References

- [1] Mrinal Sarkar and Neelima Gupte. Phase synchronization in the two-dimensional Kuramoto model: Vortices and duality. *Physical Review E*, 103(3), 3 2021.
- [2] S. Strogatz, D. Abrams, A. McRobie, et al. Crowd synchrony on the millennium bridge. *Nature*, 438:43–44, 2005.
- [3] Juan A. Acebrón, L. L. Bonilla, Conrad J. Pérez Vicente, Félix Ritort, and Renato Spigler. The Kuramoto model: A simple paradigm for synchronization phenomena. *Reviews of Modern Physics*, 77(1):137–185, 1 2005.
- [4] Renze Dijkhuizen. BEP Kuramoto model. <https://github.com/Renzed/BEP>, 2021.
- [5] Andreas Rößler. Strong and Weak Approximation Methods for Stochastic Differential Equations—Some Recent Developments. In *Recent Developments in Applied Probability and Statistics*, pages 127–154. 2010.
- [6] Vigirdas. Mackevicius. *Introduction to stochastic analysis: integrals and differential equations*. ISTE Ltd, 2011.
- [7] Steven H Strogatz. From Kuramoto to Crawford: exploring the onset of synchronization in populations of coupled oscillators. *Physica D*, 143:1–20, 2000.
- [8] K Binder. Condensed Finite Size Scaling Analysis of Ising Model Block Distribution Functions. *Z. Phys. B-Condensed Matter*, 43:119–140, 1981.
- [9] Mrinal Sarkar. Noise-induced synchronization in the kuramoto model on finite 2d lattice, 2020. [arXiv:2004.00294](https://arxiv.org/abs/2004.00294) [nlin.AO].
- [10] Hyunsuk Hong and Lei-Han Tang. Anomalous Binder Cumulant and Lack of Self-averageness in Systems with Quenched Disorder. *Korean Physical Society*, 2006.
- [11] Steven H Strogatz and Renato E Mirollo. Phase-locking and critical phenomena in lattices of coupled nonlinear oscillators with random intrinsic frequencies. *Physica D*, 31:143–168, 1988.
- [12] J. Ochab and P. F. Góra. Synchronization of coupled oscillators in a local one-dimensional kuramoto model, 2009. [arXiv:0909.0043](https://arxiv.org/abs/0909.0043) [nlin.AO].
- [13] Kaihua Xi, Johan L. A. Dubbeldam, and Hai Xiang Lin. Synchronization of cyclic power grids: Equilibria and stability of the synchronous state. *Chaos: An Interdisciplinary Journal of Nonlinear Science*, 27(1):013109, Jan 2017.
- [14] P. C. Hohenberg. Existence of Long-Range Order in One and Two Dimensions. *Phys. Rev.*, 158(383), 1967.
- [15] N. D. Mernin and H. Wagner. Absence of Ferromagnetism or Antiferromagnetism in One- or Two-Dimensional Isotropic Heisenberg Models. *Phys. Rev. Lett.*, 17(1133):135, 1966.
- [16] J.M. Thijssen. LECTURE NOTES STATISTICAL PHYSICS AP3021, 2018.

Appendix

Proof of the Binder cumulant limit

We first look at the case where the oscillators are $U(0, 2\pi)$ i.i.d. Then first note that $\langle e^{ik\theta} \rangle = 0$ for $k \in \mathbb{Z} \setminus \{0\}$. We work out the second moment:

$$\begin{aligned} \langle r^2 \rangle &= \frac{1}{N^2} \cdot \left(\left(\sum_j e^{i\theta_j} \right) \left(\sum_k e^{-i\theta_k} \right) \right) \\ &= \frac{1}{N^2} (N \cdot \langle e^0 \rangle + N(N-1) \cdot \langle e^{i\theta} \rangle \langle e^{-i\theta} \rangle) \\ &= \frac{1}{N} \end{aligned}$$

Further, we work out the fourth moment:

$$\begin{aligned} \langle r^4 \rangle &= \frac{1}{N^4} \left(\left(\sum_j e^{i\theta_j} \right) \left(\sum_k e^{i\theta_k} \right) \left(\sum_l e^{-i\theta_l} \right) \left(\sum_m e^{-i\theta_m} \right) \right) \\ &= \frac{1}{N^4} \left(N(N-1)(N-2)(N-3) \langle e^{i\theta} \rangle^2 \langle e^{-i\theta} \rangle^2 \right. \\ &\quad + N(N-1) \left(\langle e^{2i\theta} \rangle \langle e^{-2i\theta} \rangle + 2 \langle e^0 \rangle^2 \right) \\ &\quad + N(N-1) \left(2 \langle e^{i\theta} \rangle \langle e^{-i\theta} \rangle + 2 \langle e^{-i\theta} \rangle \langle e^{i\theta} \rangle \right) \\ &\quad + N(N-1)(N-2) \left(\langle e^{2i\theta} \rangle \langle e^{-i\theta} \rangle^2 + 4 \langle e^{i\theta} \rangle \langle e^{-i\theta} \rangle + \langle e^{-2i\theta} \rangle \langle e^{i\theta} \rangle^2 \right) \\ &\quad \left. + N \langle e^0 \rangle \right) \\ &= \frac{1}{N^4} (2N(N-1) + N) \end{aligned}$$

We now introduce the eigenfrequencies of the oscillators which are $\mathcal{N}(0, \sigma^2)$ i.i.d. Thus, we now look at

$$r^2 = \frac{1}{N^2} \left(\left(\sum_j e^{i(\theta_j + \omega_j t)} \right) \left(\sum_k e^{-i(\theta_k + \omega_k t)} \right) \right).$$

Again we note the characteristic function $\langle e^{i\omega t} \rangle = e^{-\frac{1}{2}(\sigma t)^2}$. Through some careful bookkeeping of terms we extend our previous result to obtain the same results, but now valid for any t and σ^2 . We then combine this to find that

$$\begin{aligned} U_r &= 1 - \left[\frac{\langle r^4 \rangle}{3 \langle r^2 \rangle^2} \right] \\ &= 1 - \frac{N^{-4} (2N(N-1) + N)}{3N^{-2}} \\ &= 1 - \frac{2N(N-1)}{3N^2} - \frac{1}{3N} \\ &= 1 - \frac{2}{3} + \frac{1}{3N} \end{aligned}$$

This has a deviation of $1/3N$ from $1/3$, so for systems larger than 10 nodes we may say

$$U_r \approx \frac{1}{3}.$$

We can also ignore the initial positions and look at just the result of moving with velocities $\omega_j \sim \mathcal{N}(0, \sigma^2)$, so we look at

$$r = \frac{1}{N} \sum_j e^{i\omega_j t}.$$

We can then apply the previous work and arrive at

$$U_r = 1 - \left[\frac{N(N-1)(N-2)(N-3)e^{-2(\sigma t)^2} + N(N-1) \left(2 + 4e^{-(\sigma t)^2} + e^{-4(\sigma t)^2} \right) + N(N-1)(N-2) \left(2e^{-3(\sigma t)^2} + 4e^{-(\sigma t)^2} \right) + N}{3 \left(N^2 + 2N^2(N-1)e^{-(\sigma t)^2} + N^2(N-1)^2e^{-2(\sigma t)^2} \right)} \right].$$

We can write this a bite more shorthand using big \mathcal{O} notation

$$U_r = 1 - \left[\frac{2N^2 - N + \mathcal{O}(N^4) \mathcal{O}(e^{-2(\sigma t)^2}) + \mathcal{O}(N^2) \mathcal{O}(e^{-(\sigma t)^2}) + \mathcal{O}(N^3) \mathcal{O}(e^{-(\sigma t)^2})}{3 \left(N^2 + \mathcal{O}(N^3) \mathcal{O}(e^{-(\sigma t)^2}) + \mathcal{O}(N^4) \mathcal{O}(e^{-2(\sigma t)^2}) \right)} \right].$$

Which, leaving out much more details, can be simplified even further to

$$U_r = 1 - \left[\frac{2N^2 - N + \mathcal{O}(N^4) \mathcal{O}(e^{-(\sigma t)^2})}{3 \left(N^2 + \mathcal{O}(N^4) \mathcal{O}(e^{-(\sigma t)^2}) \right)} \right].$$

It is then easy to see that the order terms decay extremely fast, resulting once again in $U_r \approx 1/3 - 1/N$ for settling times $T > 2/\sigma$.